PAGEOPH, Vol. 130, Nos. 2/3 (1989) 0033-4553/89/030463-17$1.50 + 0.20/0

Wind Fluctuations near a Cold Vortex-Tropopause Funnel System Observed by the MU Radar

SHOICHIRO FUKAO,[1] MANABU D. YAMANAKA,[2] HIROMASA MATSUMOTO,[3] TORU SATO,[1] TOSHITAKA TSUDA[1] and SUSUMU KATO[1]

Abstract—Vertical and temporal variations of three-dimensional wind velocity associated with an upper-tropospheric cold vortex-tropopause funnel system were observed by an MST radar in Japan (the MU radar). Marked changes of vertical velocity and horizontal wind direction were found between the inside and outside of the cold vortex. The vertical velocity activity outside the vortex was asymmetric; it was most active in a sector before the vortex. Unsaturated internal gravity waves in their generation stage contribute predominantly to the vertical velocity activity, suggesting that tropospheric occluded cyclones may be a possible source of middle-atmospheric gravity waves through the geostrophic adjustment process.

Key words: MST radar observation, cold vortex, tropopause funnel, internal gravity waves.

1. Introduction

Synoptic structures of the polar front and the tropopause jet stream were well analyzed, mainly based on 12-hourly rawinsonde observations before the 1970's (see, *e.g.*, PALMEN and NEWTON, 1969), which were followed by sub-synoptic-scale studies using aircraft observations (*e.g.*, SHAPIRO, 1974). It is noted among them that the occlusion of an extratropical cyclone in the lower troposphere is attended by a cold vortex (or cut-off cyclone) in the upper troposphere and also by a tropopause funnel (see Chapter 10 of PALMEN and NEWTON). This is one of the typical structures found in the final stage of a baroclinic disturbance development. However, even now, weather prediction in this stage is very difficult, partly because we do not have sufficient information on the contribution of sub-synoptic scale phenomena, which should be based on continuous high-resolution observations.

On the other hand, the most controversial problem of middle-atmospheric gravity waves is related to the wave sources. Orographic stationary waves must

[1] Radio Atmospheric Science Center, Kyoto University, Uji, Kyoto 611, Japan.
[2] Faculty of Education, Yamaguchi University, Yamaguchi-shi, Yamaguchi 753, Japan.
[3] Department of Electrical Engineering, Kyoto University, Yoshida, Kyoto 606, Japan.

break almost entirely below middle stratospheric altitudes (MATSUNO, 1982; TANAKA and YAMANAKA, 1985; ZHU and HOLTON, 1987); nevertheless, both theory and observation of the mesosphere require waves coming from some nonstationary source at the lower altitudes (see FRITTS, 1984, for a review). Since a tropospheric cyclone occlusion radiates momentum and energy through the geostrophic adjustment processes, this may be one of the major sources of middle-atmospheric internal gravity waves. In order to verify this, continuous high-resolution observations of three-dimensional wind variations associated with the frontal jet stream are necessary. In particular, the vertical velocity is more important than the horizontal velocity for gravity waves in their generation stage and/or near the wave source, which is the opposite case as for inertio-gravity waves near their critical levels [see (A9) in Appendix].

The MU radar (a VHF-band MST radar at Shigaraki, Japan; 34.85°N, 136.10°E) has recently started frontal phenomenon observations (WAKASUGI *et al.*, 1985; FUKAO *et al.*, 1988). This technique provides three-dimensional wind data from the middle troposphere through the lower stratosphere with far higher resolution in both time ($\sim$1 min) and altitude ($\sim$150 m) than was previously possible by conventional meteorological instruments. Both meridional-vertical circulation near the frontal surface and individual cloud convection can be observed by this powerful technique. The previous observations by the MU radar were made over a typical "axi-symmetric" front (symmetric with respect to the earth's rotation axis) in the Baiu season (FUKAO *et al.*, 1988).

In this paper we show results of a typical cold vortex-tropopause funnel system observed on 3–7 June, 1985. Details of the radar system and observational technique can be found in FUKAO *et al.* (1985a,b) and SATO *et al.* (1985). The full capabilities of the MU radar have been employed since November 1984, and the reliability and continuity of data shown in this paper are much improved from the previous observations.

2. *Synoptic-scale Situations*

In this section we show the synoptic-scale features during the period of the MU radar observation, based on the 6-hourly observations of wind, temperature, pressure, geopotential height and humidity by the Japan Meteorological Agency (JMA, 1986) and the 12-hourly objective analyses of JMA (1983, 1985a,b).

Figures 1a–c show the frontal contours, tropopause height contours and the isotherms at the 250 hPa level (10–11 km), respectively, at 0900 LST (0000 UT) 6 June, 1985. Clearly we find typical structures of the cold vortex and tropopause funnel. The locations of the lowest tropopause height (center of the funnel) and the lowest temperature are not the same; the latter is also shifted from the center of vortex motion at the same level (not shown). The streamlines (geopotential height

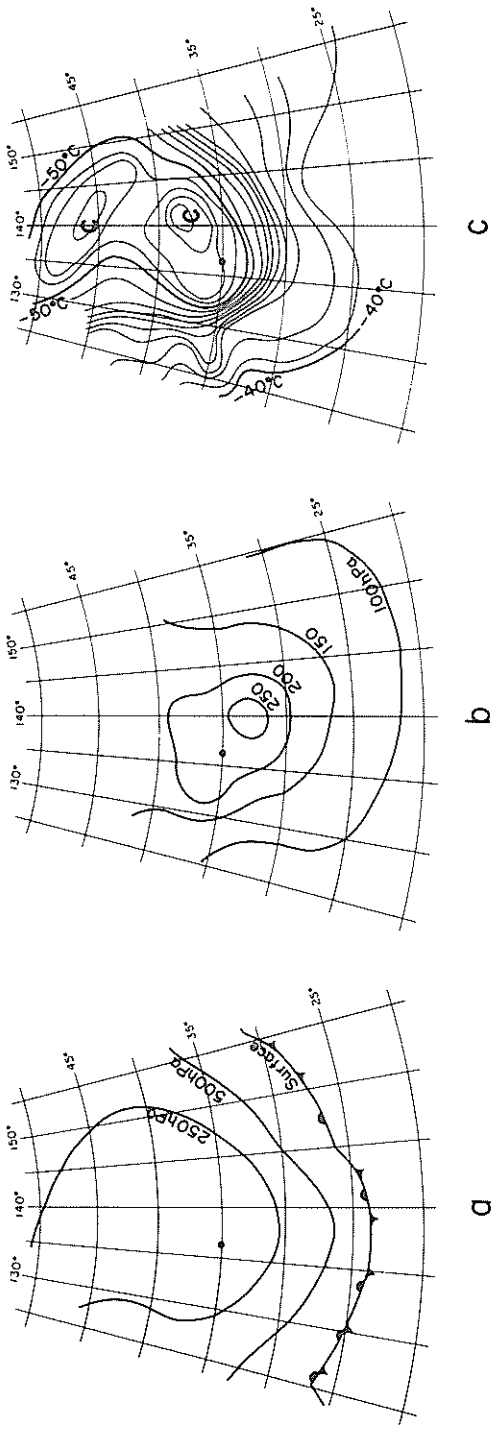

Figure 1
(a) Frontal contours, (b) tropopause height contours, and (c) 250-hPa isotherms at 09 LST 6 June, 1985, based on JMA (1985b, 1986). The location of the MU radar is indicated by the dot.

contours) are, in general, not parallel with the isotherms, and the temperature over the tropopause funnel center is not a minimum but is highest at stratospheric altitudes, which will be confirmed later.

In Figure 2 the geopotential height contours and isotherms are plotted in time-latitude cross-sections at 400, 200, and 100 hPa (7, 12 and 16 km). The lowest temperature appears to the north of the MU radar at 200 hPa, which is consistent with the 250 hPa chart of Figure 1c. However, in the 400 hPa chart of Figure 2, the lowest temperature appears to the south of the radar. Thus, the lowest temperature shifts southwards with decreasing altitude. The geopotential height contours in Figure 2 show that the center of the vortex motion also shifts southwards as the altitude decreases. Based on these features, we conclude tentatively that the

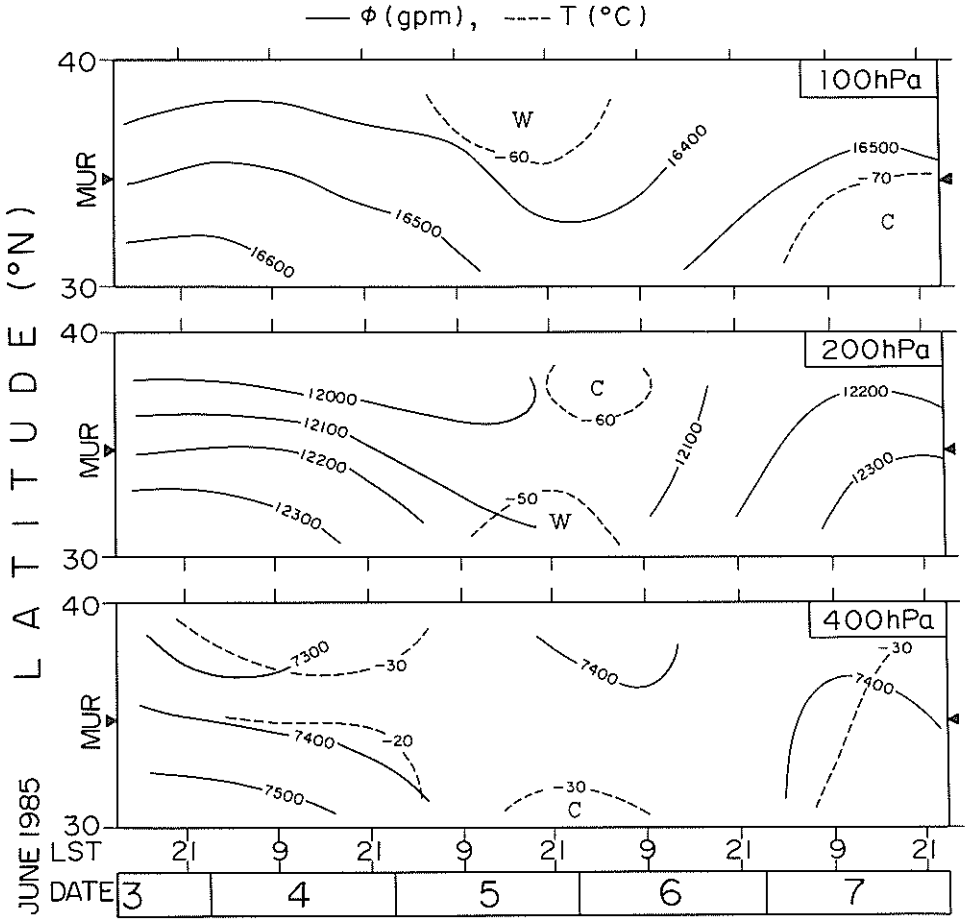

Figure 2
Time-latitude cross-sections of geopotentials and temperatures on the 100-, 200- and 400-hPa pressure surfaces, based on JMA (1983, 1985a,b, 1986).

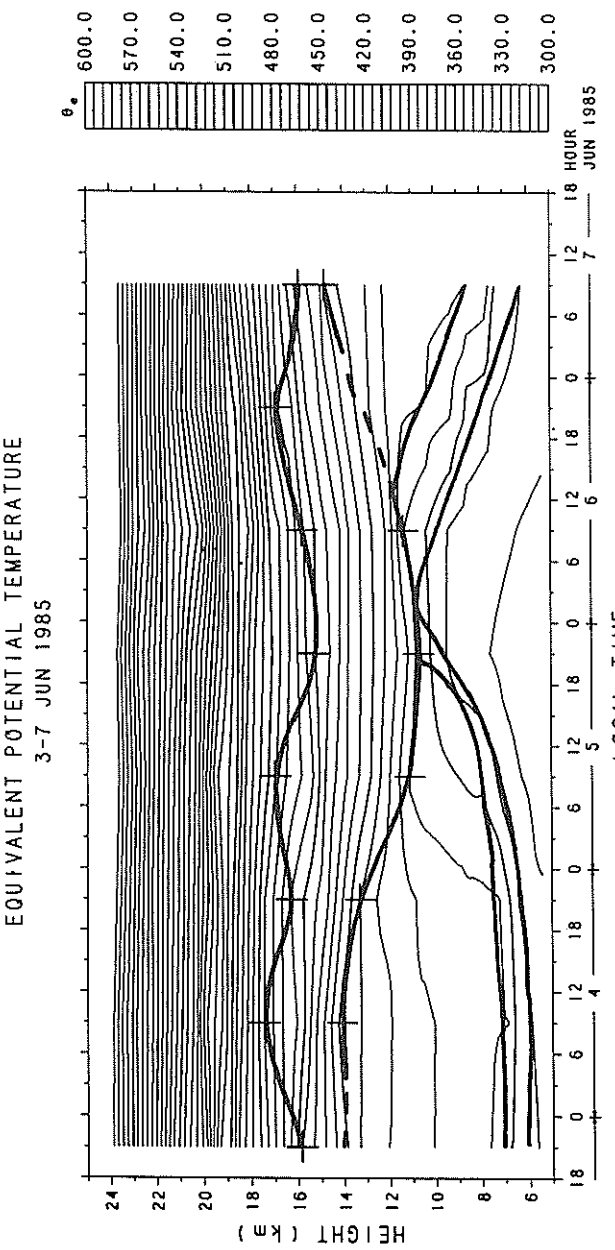

Figure 3
Time-altitude cross-section of equivalent potential temperature at Shionomisaki, based on JMA (1986). Thick curves are the tropopauses and frontal surfaces.

center of the cold vortex (lower than the 10 km altitude) passed south of the radar on 5–6 June.

Figure 3 shows the pseudo-adiabats in a time-altitude cross-section over Shionomisaki (33.45°N, 135.77°E; about 150 km south of the MU radar). There are two tropopauses throughout the observational period; the higher one located at 16–17 km altitude is continued equatorward whereas the lower one at 10–14 km extends poleward. We can reconfirm in this figure that the temperature at a specific altitude is lowest in the tropospheric cold vortex while it is highest in the tropopause funnel, and that the system passed by the radar on 5–6 June.

Figure 4 shows models of the tropospheric wind variations expected to be observed by the MU radar, following the synoptic studies on a cold vortex as summarized in PALMEN and NEWTON (1969). We consider here two alternative cases: the vortex center passes either north or south of the MU radar. Particularly note that the observed zonal wind direction inside the cold vortex is reversed between the two cases (see the two panels at the bottom of Figure 4). Namely, in the case that the cold vortex passes south of the radar, as tentatively concluded above, we would expect to observe easterlies inside the vortex region.

These synoptic studies on the atmospheric motions, in general, enable us to observe and predict the horizontal wind variations only. However, by using the MU radar, we can also observe the vertical velocity field which, as mentioned before, cannot be disregarded, and is possibly more important than the horizontal wind variation in discussing the generation stage of internal gravity waves. This is an important result of the present paper.

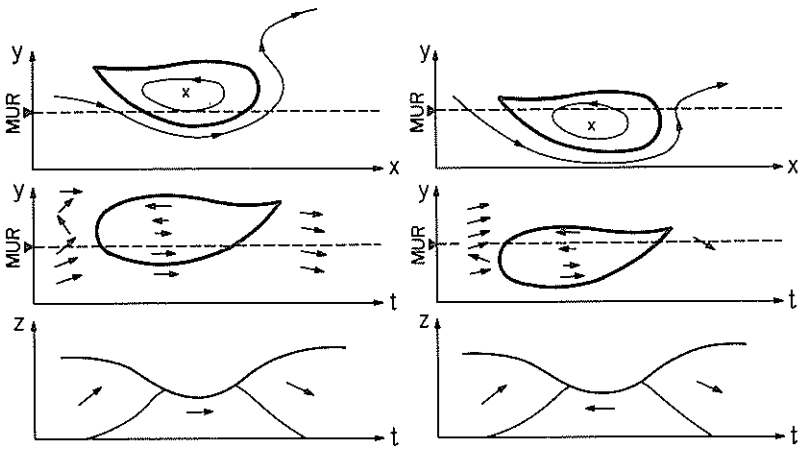

Figure 4

Model of a cold vortex (top; the vortex center is indicated by a cross) and corresponding wind distributions at the MU radar latitude (middle and bottom). The left and right columns are the cases where the cold vortex center passes north and south of the MU radar, respectively. Arrows indicate zonal-meridional winds expected by the model. Symbols x, y, z and t denote eastward, northward and upward directions and time, respectively.

3. MU Radar Observations

Figure 5 shows the variations of three-dimensional wind velocity observed by the MU radar on 3–7 June, 1985. The horizontal wind changes its direction in the vicinity of the frontal surface shown in Figure 3. In particular, we find a clear reversal of the horizontal wind direction between the outside and inside of the cold vortex (below the lower tropopause). Comparing Figure 5a with Figure 4, this fact is quite consistent with the case that the vortex center passes south of the radar. The wind variation inside the cold vortex is relatively weak, which suggests a rather stable stratification. Although there is a change of horizontal wind direction between the outside and inside of the tropopause funnel, this change is not so strong as to reverse the zonal component completely. These features are well confimed by vertical shears of the horizontal wind shown in Figure 6.

We notice in Figure 5 that the three-dimensional wind in the sector before the passage of the cold vortex (3–5 June) is quite different from that in the sector after the passage of the cold vortex (6–7 June). First of all, the vertical velocity field is more active before the cold vortex and calmer after it. If the sector before the cold vortex has a character like a warm front in the lower-tropospheric levels, this sector may be less stable because of the warmer-air advection from the south of the vortex. The variations of vertical velocity in the preceding sector take wavy or cell-like structures on a time scale of several hours.

Strong downdrafts (maximum speed ~ 0.5 m/s) were observed at altitudes lower than 16 km on the afternoon of 4 June, but their concrete interpretation has not yet been given. In the previous observation over the Baiu front, FUKAO *et al.* (1988) suggested the existence of updraft events of 22-hour intervals. We find a similar feature also in the present observation; updrafts of ~ 0.2 m/s appeared at altitudes below 10 km at ~ 18 LST 5 June, 15 LST 6 June and ~ 12 LST 7 June. Although this feature is much more disturbed than in the previous observation by the vertical velocity activity asymmetric to the cold vortex, the coincidence of the updraft intervals in the two observations should be noted.

Furthermore, we can find a strong northerly at upper-tropospheric altitudes in the sector after the cold vortex. This may be caused by a tropopause jet stream curving around the cold vortex. This is, in general, consistent with the results of the aforementioned synoptic studies (see PALMEN and NEWTON, 1969).

In the above we have considered phenomena with time scales larger than several hours, since Figure 5 shows velocity vectors averaged over ~ 1 hour. The wind velocity activity in the period after the cold vortex seems calmer in Figure 5, but it involves some phenomena with smaller time scales. So we replot the wind velocity variations during this period in the similar cross-sections with a higher time resolution (~ 15 min) (see Figure 7). An interesting feature of weak up- and down-drafts with cell-like patterns is found inside the cold vortex below the frontal surface bordering the sector behind the vortex (see also Figure 7). The amplitudes of these vertical motions are not strong (~ 0.2 m/s), but their

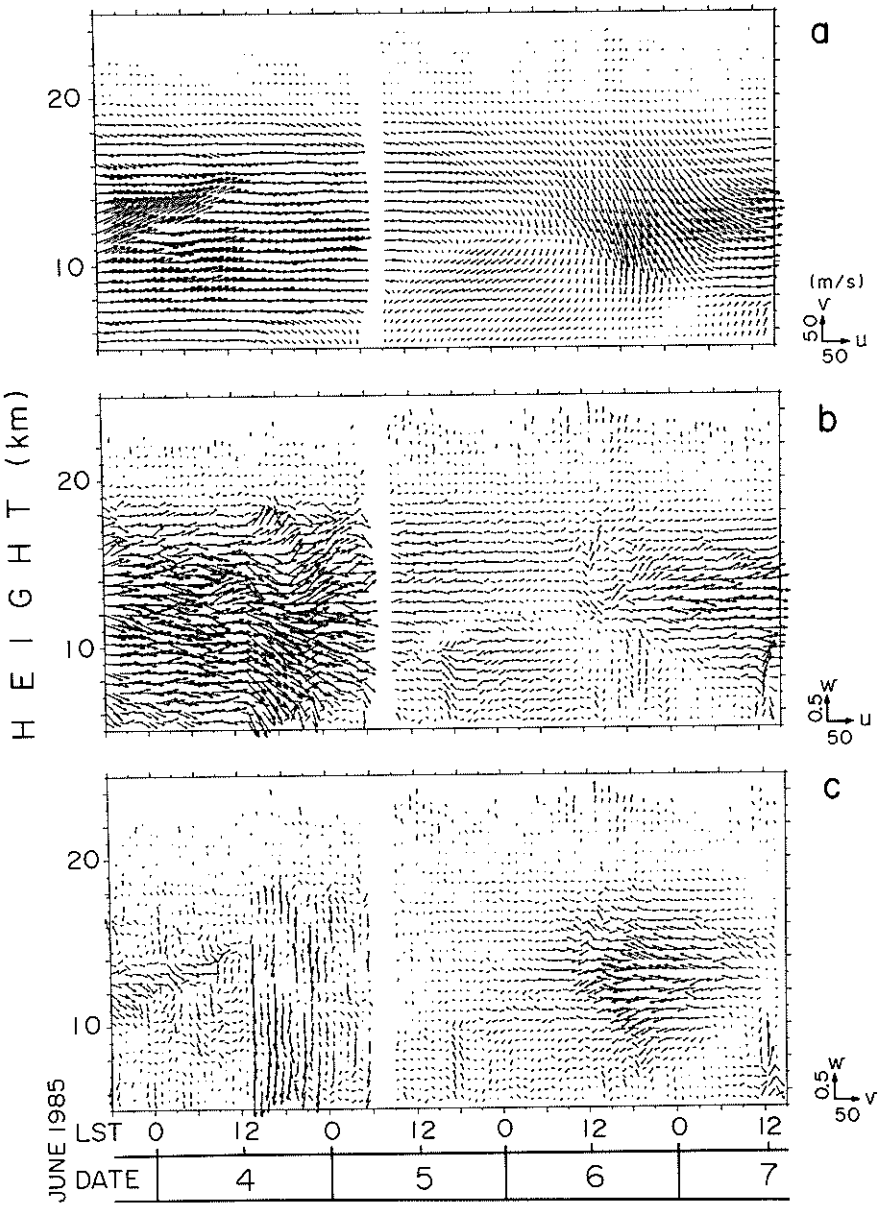

Figure 5

Time-altitude cross-sections of (a) zonal-meridional, (b) zonal-vertical, and (c) meridional-vertical winds. Scales are indicated near the bottom right corner of each frame. Symbols u, v and w denote eastward, northward and upward winds, respectively. Winds are averaged over ~1 hour.

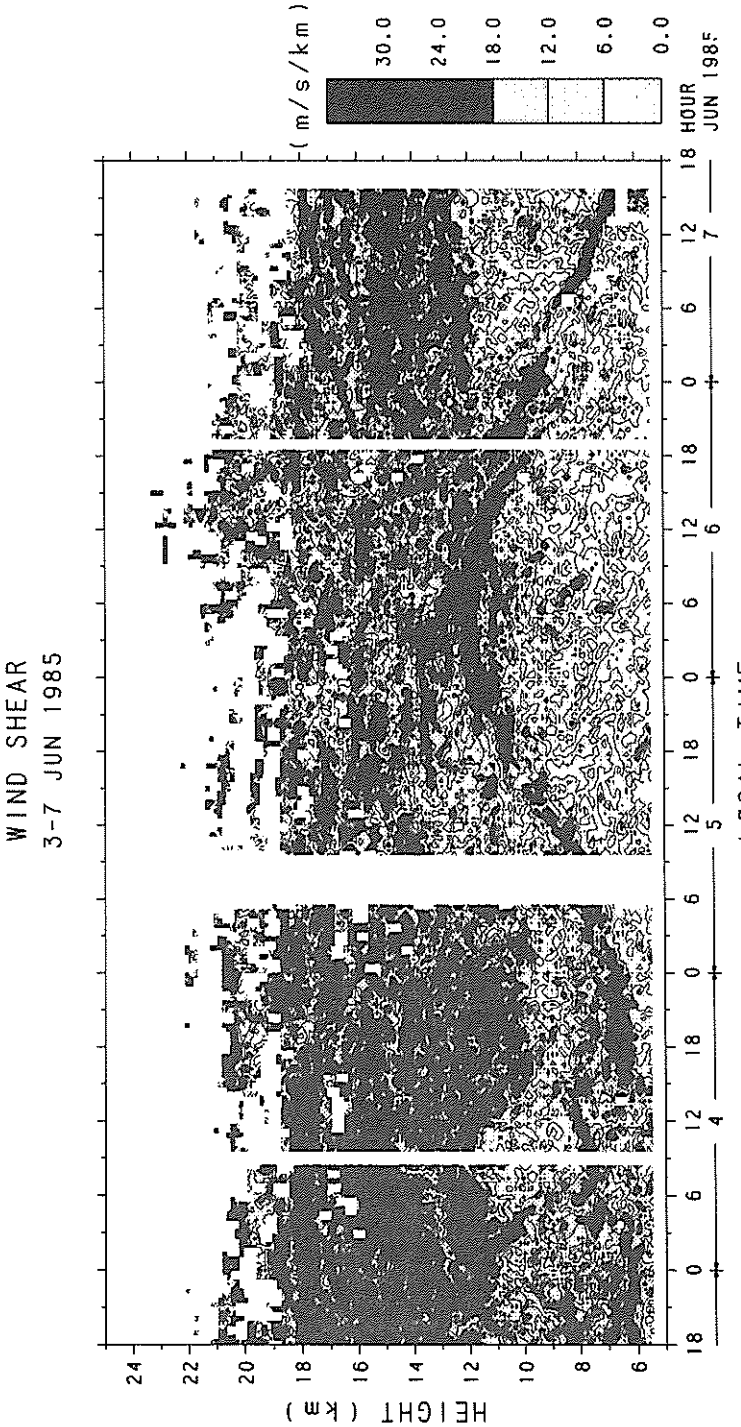

Figure 6
Time-altitude cross-section of the vertical shear of horizontal wind. The contours are drawn at 6 m/s/km intervals.

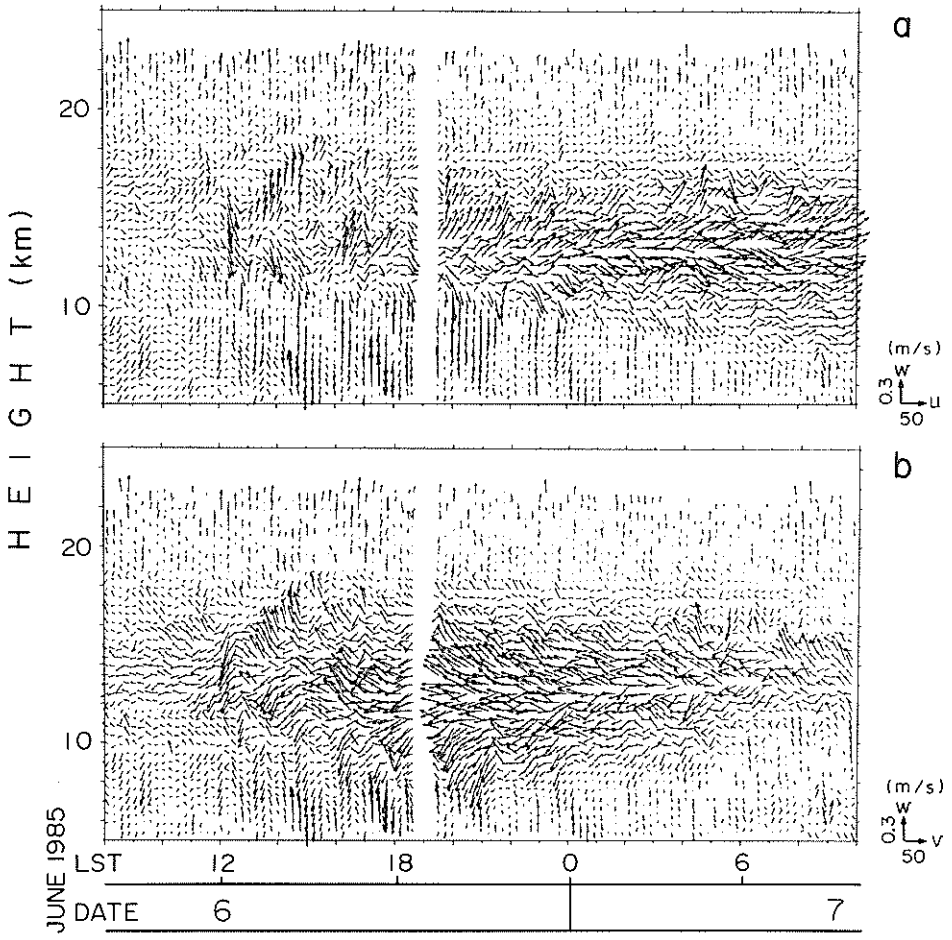

Figure 7
Time-altitude cross-sections of (a) zonal-vertical and (b) meridional-vertical winds in the sector after the passage of the cold vortex-tropopause funnel system. Winds are averaged over ~15 min.

temporal behaviors are highly systematic. The time scale of this cell-like structure is ~1 hour.

Figure 8 shows the distributions of echo power and echo power ratio. Strong echoes are distributed surrounding the cold vortex. They correspond well with the strong stratifications and shears (Figures 3 and 6) as demonstrated in detail by TSUDA *et al.* (1988). Thus severe turbulence may be induced by shear instabilities (*e.g.*, Kelvin-Helmholtz billows) rather than convective ones. Comparing Figures 8a and b, we suppose that the turbulence in the troposphere is principally on the curved plane surrounding the cold vortex, and that the turbulence in the stratosphere is embedded in thin horizontal layers induced by inertio-gravity wavefronts.

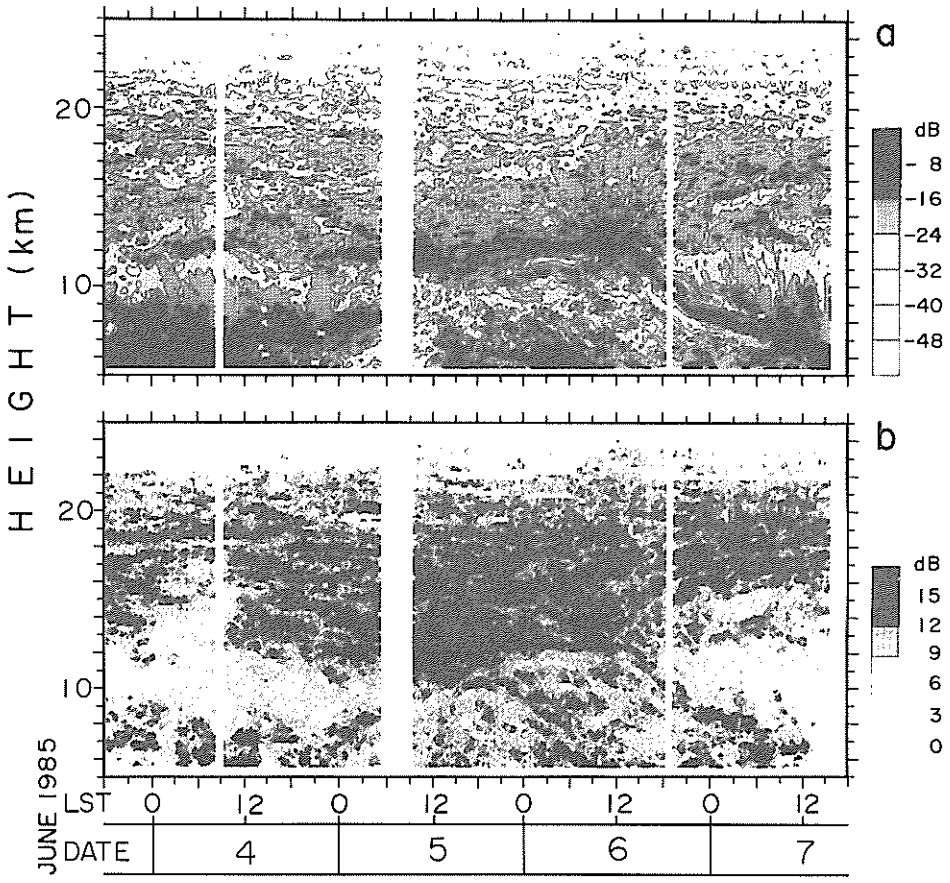

Figure 8
Time-altitude cross-sections of (a) the vertical echo power intensity and (b) the intensity ratio of vertical echo to off-vertical echo (10° off the zenith). In the former, the intensity is in an arbitrary unit, and contours are drawn at 8 dB intervals. In the latter, the contours are drawn at 3 dB intervals.

4. *Discussion of the Vertical Velocity Field*

In order to discuss the mesoscale atmospheric motions more quantitatively, we analyze the vertical-wavenumber (m) spectra $F_w(m)$ of the vertical velocity (w) for an altitude range of 6–20 km. The observed horizontal velocity (u) is highly modulated by synoptic-scale structures of the cold vortex-tropopause funnel system, and so we do not show horizontal velocity spectra $F_u(m)$. As mentioned in Section 1 and also described in (A9) of the Appendix, $F_w(m)$ becomes more important than $F_u(m)$ in discussing the generation stage of internal gravity waves.

Figure 9 gives some "area-preserving" spectra $m \cdot F_w(m)$ which are useful for evaluation of the relative contributions of each wavenumber component to the

variance or mean-square fluctuation of a physical quantity (*cf.*, BRETHERTON *et al.*, 1969). $m \cdot F_w(m)$ monotonically increases as m approaches the minimum in the observed range. This indicates that the components with vertical wavelengths longer than several kilometers ($m \lesssim 10^{-3}\,\mathrm{m}^{-1}$) contribute predominantly to the vertical velocity fluctations. In an average, $m \cdot F_w(m)$ has an approximated slope of m^{-1}, hence $F_w(m)$ is close to a -2 power law for m. These features of $F_w(m)$ differ from the so-called "universal" features of $F_u(m)$ in a similar range of m (*e.g.*, SMITH *et al.*, 1987).

In the quasi-monochromatic theory described in the Appendix, the m^{-2} law of $F_w(m)$ corresponds to *unsaturated* internal gravity waves [see (A4)]. Such unsaturated waves may coexist with saturated waves which have a similar value of m and different values of frequency and/or horizontal wavenumber. The former dominates the latter in the w field whereas the latter becomes predominant over the former in the u field, because $|u|/|w|$ becomes larger and smaller for saturated and unsaturated

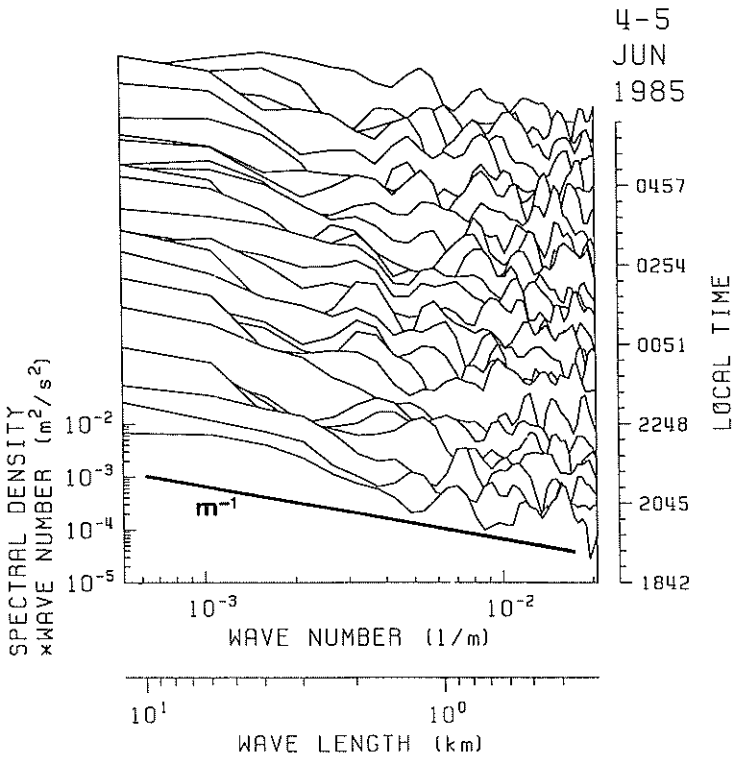

Figure 9

Examples of the "area-preserving" vertical wavenumber spectra of vertical velocity. Each spectral curve is an average of twelve approximately 2-min spectra, and it is successively multiplied by a factor of 2 to be spaced according to the right-hand side ordinate. The intensity scale is correct for the lowest spectral curve.

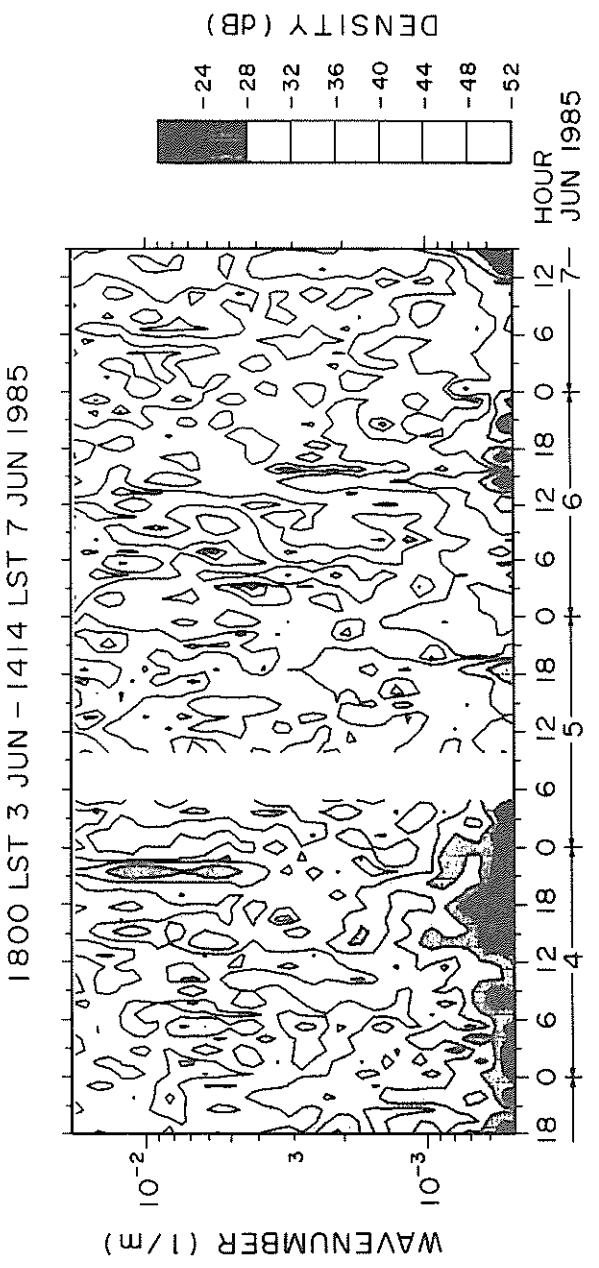

Figure 10
Temporal variation of the "area-preserving" vertical wavenumber spectra of vertical velocity for the whole observational period. Contours are drawn at 4 dB intervals.

waves, respectively. Therefore, the feature of $F_w(m)$ presented here is not inconsistent with the predominance of saturated waves universally found in $F_u(m)$. For the same reason, unsaturated gravity waves hardly appear in the hodograph analyses used in the accompanying paper (YAMANAKA *et al.*, this issue).

Figure 10 shows the temporal variation of $m \cdot F_w(m)$. It is observed that the spectral density increases on 4–5 June, that is, just before the cold vortex-tropopause funnel system passed by. Therefore, we can consider that the activity of internal gravity waves in the unsaturated stage is also asymmetric between the regions before and after the system; it is stronger before the system. Detailed considerations of the unsaturated wave generation and coexistence of the saturated and unsaturated waves (possibly including some interactions between both types of waves) should be made, but they are beyond the scope of the present paper.

5. Conclusion

Figure 11 shows a tentative model of the cold vortex-tropopause funnel system observed here. The most interesting feature is that the tropospheric vertical motions induced by unsaturated gravity waves are more active in the region before the passage of the system whereas they are less active after the passage of the system. This seems very important for discussing the mesoscale motions organized in synoptic-scale baroclinic disturbances. In the middle and lower troposphere, considerable energy may be supplied into the synoptic-scale system, possibly through cloud convection. On the other hand, at the top of the troposphere, both momentum and energy may be emitted by gravity waves through the geostrophic adjustment processes. Stratospheric inertio-gravity waves might be much amplified by this mechanism (*cf.*, YAMANAKA *et al.*, this issue).

Such an asymmetric structure should be studied in the future in relation to the nonlinear stage of tropospheric baroclinic disturbances, and also to the nonorographic source of middle-atmospheric gravity waves. The present paper has shown one vivid example to prove the importance of the MST radar technique for these meteorological studies.

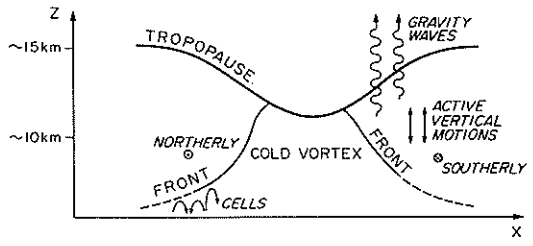

Figure 11
A tentative model of the cold vortex-tropopause funnel system. See text for details.

Acknowledgements

The Numerical Prediction Division of the Japan Meteorological Agency kindly permitted us to use their charts and technical reports of routine objective analyses for Figures 1 and 2. Special thanks are given to P. T. May, W. L. Oliver, Jr., and J. P. McClure for their careful reading of the manuscript, and to the anonymous reviewers whose comments improved the paper. The MU radar belongs to and is operated by the Radio Atmospheric Science Center of Kyoto University.

Appendix
A Brief Description of Quasi-monochromatic Gravity Wave Spectra

Monochromatic waves are derived as solutions of a homogeneous perturbation equation for steady, uniform waveguides. Although the actual atmosphere is unsteady and nonuniform, the solutions are quasi-monochromatic when the temporal and spatial variations are sufficiently slow so that the WKB approximation is valid. Such a situation for the wave field has been considered by YAMANAKA (1985) and SMITH *et al.* (1987).

At first, we consider a simple *unsaturated* noninertial gravity wave, of which the vertical velocity perturbation w is derived under the WKB approximation as

$$|w| \propto |m|^{-1/2} \propto |\hat{\omega}|^{1/2} \tag{A1}$$

with the dispersion relation

$$|m| = \frac{|k|}{|\hat{\omega}|} \cdot N, \tag{A2}$$

where $\hat{\omega}$, k and m are the intrinsic frequency, horizontal and vertical wavenumbers, respectively. N is the Väisälä-Brunt frequency. From the Boussinesq' continuity equation (density conservation) we can write the horizontal velocity perturbation u as

$$|u| = \frac{|m|}{|k|} \cdot |w|. \tag{A3}$$

We symbolize a functional form of the power spectral density as $F_\psi(\nu)$, where ψ is a physical quantity and ν is one of the wave parameters $\hat{\omega}$, k and m. In general, we can write $F_\psi(\nu) \propto \partial|\psi|^2/\partial|\nu|$, where $|\psi|^2$ corresponds to the variance or mean-square of ψ in an adequate bandwidth of ν. Then the power spectral density for vertical velocity, as a function of the vertical wavenumber, $F_w(m)$, is derived from (A1)

$$F_w(m) \propto \frac{\partial|w|^2}{\partial|m|} \propto |m|^{-2}. \tag{A4}$$

Similarly, using (A1)–(A3), we have

$$F_u(m) \propto \frac{\partial |u|^2}{\partial |m|} \propto |m|^0 = \text{const.} \tag{A5}$$

Next we consider a *saturated* (or breaking) wave. (A2) and (A3) still hold but the wave amplitude is damped from (A1). In the case of local convective (or nonlinear) saturation, the wave amplitude is given by the saturation condition

$$|k| \cdot |\xi| = |m| \cdot |\zeta| = 1 \tag{A6}$$

where $\xi = \int^t u\, dt$ and $\zeta = \int^t w\, dt$ are the horizontal and vertical displacements, respectively (YAMANAKA and TANAKA, 1984). Considering that $|u| = |\hat{\omega}| \cdot |\xi|$ and $|w| = |\hat{\omega}| \cdot |\zeta|$, (A6) can be rewritten as

$$|k| \cdot |u| = |m| \cdot |w| = |\hat{\omega}|, \tag{A6}'$$

which is the same form as that derived originally by ORLANSKI and BRYAN (1969) for an external gravity wave on ocean surface.

Using (A6)′, we have

$$F_w(m) \propto \frac{\partial |w|^2}{\partial |m|} \propto |m|^{-5}, \tag{A7}$$

$$F_u(m) \propto \frac{\partial |u|^2}{\partial |m|} \propto |m|^{-3} \tag{A8}$$

for saturated quasi-monochromatic waves. YAMANAKA (1985) and SMITH *et al.* (1987) have derived (A8).

From (A2) and (A3), we have

$$\begin{aligned} &|u| \to 0 \quad \text{and} \quad |w| \to \infty \quad \text{for} \quad |\hat{\omega}| \to \infty, \\ &|u| \to \infty \quad \text{and} \quad |w| \to 0 \quad \text{for} \quad |\hat{\omega}| \to 0. \end{aligned} \tag{A9}$$

Hence, $|w|$ of a quasi-monochromatic wave in the saturation stage (small $|\hat{\omega}|$) is vanishingly small, and $|u|$ in the generation stage (large $|\hat{\omega}|$) is also small. When a saturated quasi-monochromatic wave coexists with an unsaturated wave, $F_u(m)$ approaches the saturated spectrum (A8) whereas $F_w(m)$ becomes the unsaturated one (A4).

REFERENCES

BRETHERTON, F. P., BULL, G., LINDZEN, R. S., PAO, Y.-H., REITER, E. R., and WILHELMSSON, H. (1969), *The Specral Gap*, Radio Sci. *4*, 1361–1363.

FRITTS, D. C. (1984), *Gravity Wave Saturation in the Middle Atmosphere: A Review of Theory and Observations*, Rev. Geophys. Space Phys. *22*, 275–308.

FUKAO, S., SATO, T., TSUDA, T., KATO, S., WAKASUGI, K., and MAKIHIRA, T. (1985a), *The MU Radar with an Active Phased Array System, I. Antenna and Power Amplifiers*, Radio Sci. *20*, 1155–1168.

FUKAO, S., TSUDA, T., SATO, T., KATO, S., WAKASUGI, K., and MAKIHIRA, T. (1985b), *The MU Radar with an Active Phased Array System, 2. In-House Equipment*, Radio Sci. *20*, 1169–1176.

FUKAO, S., YAMANAKA, M. D., SATO, T., TSUDA, T., and KATO, S. (1988), *Three-Dimensional Air Motions over the Baiu Front Observed by a VHF-Band Doppler Radar: A Case Study*, Mon. Wea. Rev. *116*, 281–292.

JAPAN METEOROLOGICAL AGENCY (JMA) (1983), *The Northern-Hemisphere and Fine-Mesh Numerical Prediction Models (8L NHM and 10L FLM) and Analysis System*, JMA-Numerical Computation Center Tech. Rep., No. *29*, 75 pp.

JAPAN METEOROLOGICAL AGENCY (JMA) (1985a), JMA-Numerical Prediction Division 250-, 200- and 100-mb Objective Analyses, 3–8 June, 1985.

JAPAN METEOROLOGICAL AGENCY (JMA) (1985b), Daily Weather Maps, June 1985, 242 pp.

JAPAN METEOROLOGICAL AGENCY (JMA) (1986), Aerological Data of Japan, June 1985, 247 pp.

MATSUNO, T. (1982), *A Quasi-One-Dimensional Model of the Middle Atmosphere Circulation Interacting with Internal Gravity Waves*, J. Meteor. Soc. Japan *60*, 215–226.

ORLANSKI, I., and BRYAN, K. (1969), *Formation of the Thermocline Step Structure by Large-Amplitude Internal Gravity Waves*, J. Geophys. Res. *74*, 6975–6983.

PALMEN, E., and NEWTON, C. W. (1969), *Atmospheric Circulation Systems: Their Structure and Physical Interpretation* (Academic Press) 603 pp.

SATO, T., TSUDA, T., KATO, S., MORIMOTO, S., FUKAO, S., and KIMURA, I. (1985), *High-Resolution MST Observations of Turbulence by Using the MU Radar*, Radio Sci. *20*, 1452–1460.

SHAPIRO, M. A. (1974), *A Multiple-Structured Frontal Zone Jet Stream System as Revealed by Meteorologically Instrumented Aircraft*, Mon. Wea. Rev. *102*, 244–253.

SMITH, S. A., FRITTS, D. C., and VANZANDT, T. E. (1987), *Evidence for a Saturated Spectrum of Atmospheric Gravity Waves*, J. Atmos. Sci. *44*, 1404–1410.

TANAKA, H., and YAMANAKA, M. D. (1985), *Atmospheric Circulation in the Lower Stratosphere Induced by the Mesoscale Mountain Wave Breakdown*, J. Meteor. Soc. Japan *63*, 1047–1054.

TSUDA, T., MAY, P. T. SATO, T., KATO, S., and FUKAO, S. (1988), *Simultaneous Observations of Reflection Echoes and Refractive Index Gradient in the Troposphere and Lower Stratosphere*, Radio Sci. *23*, 655–665.

WAKASUGI, K., FUKAO, S., KATO, S., MIZUTANI, A., and MATSUO, M., (1985), *Air and Precipitation Particle Motions within a Cold Front Measured by the MU VHF Radar*, Radio Sci., *20*, 1233–1240.

YAMANAKA, M. D. (1985), *The Power Spectrum of Internal Gravity Waves: Stratospheric Balloon Observations and Interpretations*, WRI-MAP Research Note-6, Water Research Institute, Nagoya University, 13 pp.

YAMANAKA, M. D., FUKAO, S., MATSUMOTO, H., SATO, T., TSUDA, T., and KATO, S. (1988), *Internal Gravity Wave Selection in the Upper Troposphere and Lower Stratosphere Observed by the MU Radar*, Pure Appl. Geophys., *130* (2/3), 481–495.

YAMANAKA, M. D., and TANAKA, H. (1984), *Multiple "Gust Layers" Observed in the Middle Stratosphere*, in *Dynamics of the Middle Atmosphere* (eds. J. R. Holton and T. Matsuno) (TERRAPUB/D. Reidel) pp. 117–140.

ZHU, X., and HOLTON, J. R. (1987), *Mean Fields Induced by Local Gravity-Wave Forcing in the Middle Atmosphere*, J. Atmos. Sci. *44*, 620–630.

(Received August 31, 1987, revised/accepted February 1, 1988)